

An Initial Concept of A Resonance Phase Matched Junction-Loaded Travelling Wave Parametric Tripler

B-. K. Tan

Abstract—In this paper, we investigate the possibility of utilising a tunnel-junction loaded transmission line as high efficiency parametric frequency multiplier. Through the interaction between the injected primary tone and the nonlinear medium, higher harmonic tones can be generated through wave-mixing process. Here, we aim to maximise the third harmonic wave generation. We first establish a theoretical framework outlining the mechanism for generating the third harmonic component from a single pump wave propagating in a nonlinear transmission line. We begin by demonstrating that strong third harmonic generation is possible with the resonance phase matching technique, albeit with an extremely narrow operational bandwidth. To broaden the bandwidth, we modify the dispersion engineering element of our circuit and show that broadband operation is achievable, while preventing unwanted harmonic tone growth. We extend this calculation from the microwave to the millimetre and sub-millimetre regimes and demonstrate that by adjusting the parameters of the junctions and the dispersion engineering circuits, we can achieve high conversion efficiency close to 1 THz.

Index Terms—Superconductor-Insulator-Superconductor (SIS), Heterodyne Mixers, Focal Plane Array, Circular Waveguide, Probe Antenna

I. INTRODUCTION

GENERATION of high spectral purity tones at high frequencies with high output power and low noise properties is crucial for many applications, particularly for generating the local oscillator (LO) signal for astronomical millimetre (mm) and sub-millimetre (sub-mm) heterodyne receivers. Traditionally, this is achieved through a chain of frequency multipliers utilising semiconductor Schottky diodes [1], [2] in a waveguide structure in conjunction with a microwave source, for operation below 2 THz. However, these multipliers are often bulky, power-hungry, dissipate significant heat, and require complex optical arrangements for injection into the main detector mounted in the cryogenic stage, limiting their use in ultra-sensitive experiments. For higher frequency operation, a quantum cascade laser [3], [4] is generally preferred, albeit with limited tunability, lower power output, higher heat dissipation, and slightly inferior spectral purity. Other methods, such as beating two infrared lasers with photodiode [5], utilising plasmonic resonance of superconducting tunnel junctions [6], or using distributed superconductor-insulator-superconductor (SIS) mixers [7], all have their pro and cons, including limitations in terms of output power, spectral purity, added noise, or bandwidth.

In this context, we propose a new mechanism using the travelling-wave parametric amplifiers (TWPAs) technology

Department of Physics (Astrophysics), University of Oxford, Denys Wilkinson Building, Keble Road, OX1 3RH, Oxford, UK. E-mail: boonkok.tan@physics.ox.ac.uk

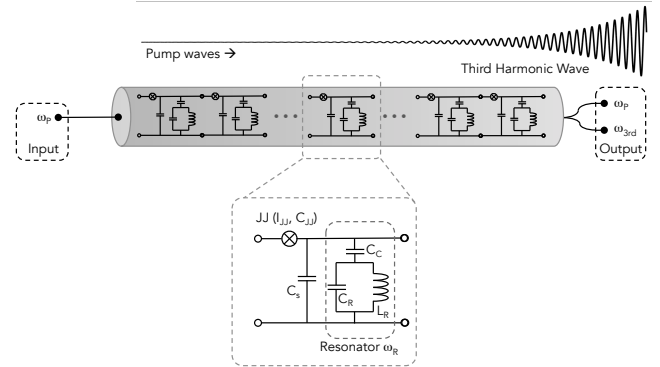


Fig. 1. Resonantly phase-matched travelling wave parametric tripler. Third harmonic photons are generated and amplified through a nonlinear interaction with the strong input pump wave as they propagate along the transmission line with a lattice period of $a = 10 \mu\text{m}$. In each unit cell, a capacitively-shunt Josephson junction (the nonlinear inductors) is capacitively coupled to an LC resonators. The circuit parameters are $C_j = 280 \text{ fF}$, $L = 100 \text{ pH}$, $C_s = 50 \text{ fF}$, $C_c = 10 \text{ fF}$, $C_R = 7.036 \text{ pF}$, $L_R = 100 \text{ pH}$, $x = 2000a$, and $I_0 = 3.29 \mu\text{A}$.

[8], [9] to generate mm and sub-mm wave signals. TWPAs offer the potential for low noise, stable wideband operation with minimal heat dissipation, and their compact design allows for integration with other circuit components. Mounting these high-frequency sources in-situ at the cryogenic stage near the main detector minimises noise leakage from room temperature sources. Additionally, integrating the compact high-frequency source with the main detector circuit enables a new operation regime, allowing the construction of a compact integrated heterodyne miniature receiver with an integrated LO source next to the mixer. This opens up the possibility of constructing an array with frequency tunability for each pixel, creating a multi-band heterodyne array, which was not feasible with conventional heterodyne receiver construction.

In this paper, we will first present the formulation of the framework necessary for predicting the generation of pump harmonics. Subsequently, we address the fundamental issues associated with employing existing TWPA technology for achieving broadband operation before introducing our proposed solution. We illustrate the solution using a practical microwave example, before extending the design to the mm/sub-mm regime, and demonstrate that by adjusting the parameters of the junctions and dispersion engineering circuits, we can theoretically achieve close to $1.5 \mu\text{W}$ of output power near 1 THz with a cascade of several parametric multipliers.

II. THEORETICAL MODEL

A meta-material transmission line loaded with a series of Josephson junctions has been successfully used as a travelling

wave parametric amplifier [8], [10] to generate exponentially high gain before. This is achieved by adding additional resonance circuits [11], [12], [13] along the transmission line to ensure that the total dispersion is near zero within the operational band. In this operational regime, it has been shown that third harmonic generation from the strong pump wave is negligible due to the junction resonance [11], [14]. However, when using this junction-loaded transmission line as a frequency tripler, the third harmonic phase mismatch needs to be minimised instead.

Here, we follow the treatment from [11] to derive the coupled wave equations for the travelling wave parametric multiplier (TWPm) in the tripler mode. The nonlinear wave equation for a Josephson junction loaded long transmission line depicted in Fig 1 can be described as [15]:

$$C_0 \frac{\partial^2 \phi}{\partial t^2} - \frac{a^2}{L} \frac{\partial^2 \phi}{\partial x^2} - C_j a^2 \frac{\partial^4 \phi}{\partial x^2 \partial t^2} = \frac{a^4}{2I_0^2 L^3} \frac{\partial^2 \phi}{\partial x^2} \left(\frac{\partial \phi}{\partial x} \right)^2 \quad (1)$$

Taking the ansatz that the solutions to be forward propagating waves of the form:

$$\phi = \frac{1}{2} [A_p(x) e^{i(k_p x + \omega_p t)} + A_3(x) e^{i(k_3 x + \omega_3 t)} + \text{c.c.}] \quad (2)$$

where A_m is the slowly varying amplitude, k_m is the wave vector, ω_m is the angular frequency and $m = p, 3$ representing

the pump and third harmonic tones respectively. Here, we assume that all harmonics higher than the third will be suppressed by the plasma resonance frequency cutoff of the Josephson junctions. Substitute the above expression (Eq. 2) into the nonlinear wave equation (Eq. 1) with the following approximations:

- 1) neglect the second derivatives of the slowly varying amplitudes using the slowly varying envelope approximation: $\left| \frac{d^2 A_m}{dx^2} \right| \ll \left| k_m \frac{dA_m}{dx} \right|$, and
- 2) neglect the first derivatives of the slowly varying amplitudes on the right side of the nonlinear wave equation: $\left| \frac{dA_m}{dx} \right| \ll |k_m A_m|$,

and defining the wave vector as $k_m = \frac{\omega_m \sqrt{C_0 L}}{a \sqrt{1 - C_j L \omega_m^2}}$, Eq. 1 can be simplified to:

$$\frac{-iC_0 \omega_m^2}{k_m} \frac{\partial A_m(x)}{\partial x} e^{i(k_m x + \omega_m t)} = \frac{a^4}{2I_0^2 L^3} \frac{\partial^2 \phi}{\partial x^2} \left(\frac{\partial \phi}{\partial x} \right)^2 \quad (3)$$

Replacing Eq. 2 into Eq. 3, and separating out the terms that oscillate at the pumps and the third harmonic frequencies, we get the following coupled equations:

$$\frac{\partial A_p(x)}{\partial x} - \frac{ia^4 k_p^3}{16C_0 I_0^2 L^3 \omega_p^2} [k_p^2 A_p(x)^2 A_p^*(x) + k_3(2k_p - k_3) A_p^{*2}(x) A_3(x) e^{-i\Delta_{kL} x}] = 0 \quad (4a)$$

$$\frac{\partial A_3(x)}{\partial x} - i \frac{a^4 k_p^2 k_3}{16C_0 I_0^2 L^3 \omega_3^2} [2k_3^2 A_p A_p^* A_3 - k_p^2 A_p^3 e^{i\Delta_{kL} x}] = 0 \quad (4b)$$

where $\Delta_{kL} = 3k_p - k_3$. This can be further simplified to:

$$\frac{\partial A_p(x)}{\partial x} - i\alpha_{p1} A_p(x)^2 A_p^*(x) - i\alpha_{p2} A_p^{*2}(x) A_3(x) e^{-i\Delta_{kL} x} = 0 \quad (5a)$$

$$\frac{\partial A_3(x)}{\partial x} - i\alpha_{31} A_p A_p^* A_3 + i\alpha_{32} A_p^3 e^{i\Delta_{kL} x} = 0 \quad (5b)$$

where the coupling coefficients are defined as:

$$\alpha_{p1} = \frac{a^4 k_p^5}{16C_{0,p} \omega_p^2 I_0^2 L^3}, \quad \alpha_{p2} = \frac{a^4 k_p^3 k_3 (2k_p - k_3)}{16C_{0,p} \omega_p^2 I_0^2 L^3} \quad (6a)$$

$$\alpha_{31} = \frac{a^4 k_p^2 k_3^3}{8C_{0,3} \omega_3^2 I_0^2 L^3}, \quad \alpha_{32} = \frac{a^4 k_p^4 k_3}{16C_{0,3} \omega_3^2 I_0^2 L^3} \quad (6b)$$

Solving the coupled amplitude equations by making the substitutions $A_p(x) = a_p e^{i\phi_p x}$ and $A_3(x) = a_3 e^{i\phi_3 x}$, where $\phi_p = \alpha_{p1} a_p a_p^*$ and $\phi_3 = \alpha_{31} a_p a_p^*$, we have:

$$\frac{\partial a_p}{\partial x} - i\alpha_{p2} a_p^{*2} a_3 e^{-i\Delta_k x} = 0 \quad (7a)$$

$$\frac{\partial a_3}{\partial x} - i\alpha_{32} a_p^3 e^{i\Delta_k x} = 0 \quad (7b)$$

where $\Delta_k = \Delta_{kL} + 3\phi_p - \phi_3$. If we proceed with the assumption that the third harmonic wave is much weaker than the pump wave (the undepleted pump approximation) i.e., $A_p(x) = a_p(0) e^{i\alpha_p x}$, $A_3 = a_3 e^{i\alpha_3 x}$ and $\alpha_3 =$

$\frac{a^4 k_p^4 k_3^2}{8C_{0,3} \omega_3^2 I_0^2 L^3} a_p(0) a_p^*(0)$, the above coupled amplitude equations can be solved analytically, resulting in

$$a_3 = \frac{(1 - e^{i\Delta'_k x}) \kappa}{\Delta'_k} \quad (8)$$

where

$$\Delta'_k = 3k_p - k_3 + 3\alpha_p - \alpha_3 \quad (9a)$$

$$\alpha_p = \frac{a^4 k_p^5}{16C_{0,p} \omega_p^2 I_0^2 L^3} a_p(0) a_p^*(0) \quad (9b)$$

$$\text{and } \kappa = \frac{a^4 k_p^4 k_3^2}{16C_{0,3} \omega_3^2 I_0^2 L^3} a_p^3(0). \quad (9c)$$

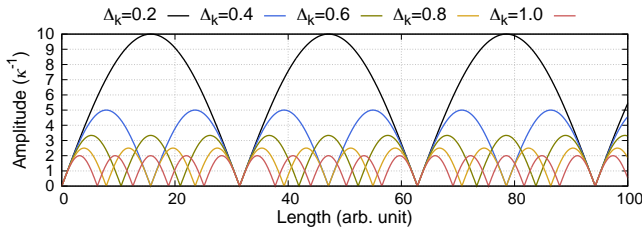


Fig. 2. Plot showing the behaviour of Eq. 8.

Eq. 8 shows that the amplitude of the third harmonic wave is periodically dependent on the length x , and the periodicity and the maximum amplitude is Δ_k dependent, as shown in Fig. 2. This means that if $\Delta_k \rightarrow 0$, then at short length, the third harmonic growth is almost linear-like. In this and the following examples, we use the circuit parameters depicted in Fig. 1. For a general case without the undepleted pump approximation, we solve Eq. 7 numerically using the Runge-Kutta method.

III. TRAVELLING WAVE PARAMETRIC TRIPLER

As shown in Eq. 8, the growth of the third harmonic wave depends heavily on Δ_k . Similar to the case of the TWPA, we can therefore utilise the resonance phase matching technique to engineer the TWPam so that $\Delta_k \rightarrow 0$. In Fig. 3 (a), we show the dispersion curve of Δ_k plotted against the input pump frequency. One immediately noted that there is a strong resonance near 30 GHz. This is due to the natural resonance of the junction $f_j = 1/2\pi\sqrt{L_j C_j}$. Another weaker resonance appears at a third of this frequency, near 10 GHz, as the third harmonic's wave vector is three times higher than the pump's wave vector. Below the 10 GHz resonance, the two sharp resonance spikes were induced by the additional resonator circuits (one seen by the pump wave and the lower frequency resonance by the third harmonic), introduced to match the total phase Δ_k . The dispersion curve near this region is zoomed in Fig. 3 (b) for clarity purposes. It is clear now that near these resonance frequencies, the conversion efficiency from the pump to the third harmonic wave increase drastically, as shown in the lower panel of Fig. 3 (a).

This can be illustrated more clearly from Fig. 4. On the bottom panels, the pump frequency was set to be away from the resonance frequency at 5.994 GHz. As can be seen, only a small amount of energy is converted to the third harmonic. However, if the pump frequency is set closer to the resonance frequency at 5.99471 GHz i.e., the total phase difference is closed to zero, one can improve the power transfer from the pump to the third harmonics significantly. This is shown in the top panels, where one can see that near $I_p \approx 0.76I_0$, the amplitude of the third harmonic wave is now higher than the pump's amplitude, meaning that more than half of the energy is now transferred to the third harmonic wave. Another important observation here is that as shown in the top right panel, the maximum power transfer is periodically oscillating along the length of the TWPam, just as predicted via Eq. 8. Noted that these plots were made without the undepleted pump approximation depicted in Eq. 7.

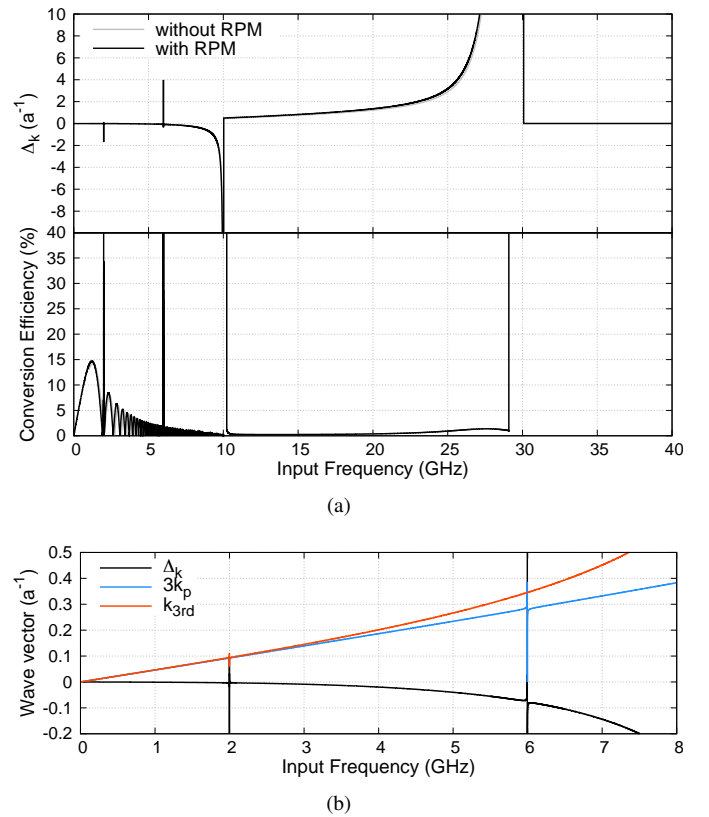


Fig. 3. (a) Top panel: Phase mismatched between the pump and the third harmonic. In this case, the junction capacitance was set to be 280 fF, $L_j = 100$ pH, giving a natural resonance at 30 GHz. This also creates a resonance at 10 GHz, a third of the natural resonance frequency, as the third harmonic wavelength is three times smaller than the pump. The two resonances created by the additional resonators are visible at 2 GHz and 6 GHz. This is zoomed in sub-plot (b) for clarity. Here, it is clearly seen that the 2 GHz resonance in the Δ_k curve was due to the wave vector k_{3rd} , while the intended 6 GHz resonance by the pump's wave vector k_p . Bottom panel: The conversion efficiency clearly shown that there are some conversion below 10 GHz, where at resonances, the corresponding Δ_k curve close to zero and the conversion efficiency improved up significantly. Above 30 GHz, Δ_k curve becomes purely imaginative, hence no conversion is possible. Note that these curve was plotted with the pump depletion assumption, but the underlying principle remains the same for the pump depletion case.

However, from Fig 3 (a), it is clear that the exponential growth of third harmonic wave only happens at a particular set of frequencies. In other words, with this configuration, the operational bandwidth is extremely narrow (note how the minute difference between the two frequencies used to plot Fig. 4 have on the conversion efficiency). In order to broaden the operational bandwidth, one can utilise a tunable planar resonance circuit (via changing the kinetic inductance of a superconducting line using bias current below the critical current) to compensate for the bandwidth performance, but this could add to the complexity of fabricating such devices.

IV. BROADBAND MICROWAVE THIRD HARMONIC GENERATOR

Nevertheless, it is easy to show that this intrinsically narrow operational bandwidth is simply due to the fact that the pump needs to be very close to the resonance frequencies, which was set with very high quality factor in the case

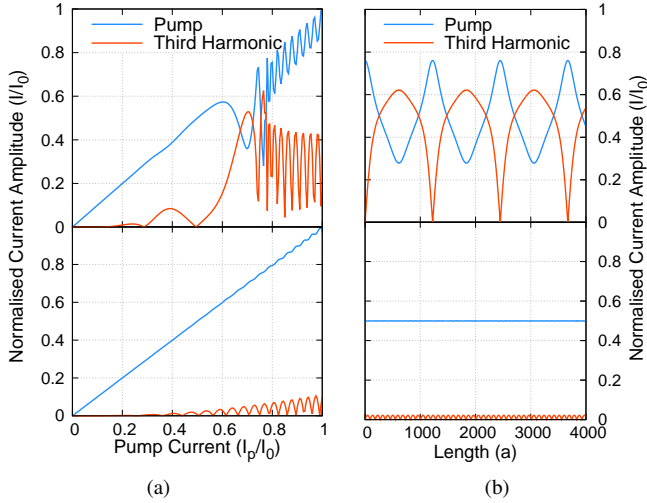


Fig. 4. (a) The normalised amplitude of the resulting pump and third harmonic wave relative to the critical current of the Josephson junction (I_0), in relation with the strength of input pump current (I_p). The bottom panel shows the case where the pump frequency is away from the resonance frequency at 5.994 GHz, while the top panel shows the case where the pump frequency is very close to the resonance at 5.99471 GHz (A similar case can be found near the 2 GHz resonance as well, but apart from that, conversion efficiency is negligible, as is clearly shown in Fig 3.). (b) The normalised amplitude of the resulting pump and third harmonic wave along the transmission line. Bottom panel shows the 5.994 GHz case, where $I_p/I_0 = 0.5$, while top panel shows the resonance case with $I_p/I_0 = 0.76$.

shown above. Therefore, in order to broaden the operational bandwidth, we can reduce the Q-factor of the resonator. As described earlier, due to the third harmonic wave generated along the transmission line, the resonator will induced a lower resonance at a third of the natural resonator frequency but flip in polarity against frequency. This in effect altered the total Δ_k value between the two resonances. If the Q-factor value is low enough, the two resonance curves overlapped at larger intermimence frequencies, and there would be a region where Δ_k is very close to zero. This is shown in the Fig. 5 (a). It is worthwhile noting that the phase relation Δ_k in this case is also rely heavily on the natural resonance of the Josephson junctions. It is therefore preferable that the junction resonance is at a higher frequency, so that the Δ_k curve is flatter near the operational frequencies region, and hence it's easier to make $\Delta_k \rightarrow 0$ at a broader bandwidth.

In the bottom panel of Fig. 5 (a), we show the conversion efficiency curve of a TWPaM using the low-Q resonators to compensate for the phase difference. As can be seen, the operational bandwidth is now much wider than the previous case with a conversion efficiency better than 40% from 4–5.5 GHz, resulting in the generation of output signal from about 12–16.5 GHz.

V. BROADBAND MILLIMETRE WAVE & THZ THIRD HARMONIC PARAMETRIC TRIPLER

In order to operate the third harmonic generator at higher frequency, it is evident that we need to shift the junction resonance much further away from the operational band, since no wave can propagate beyond the junction resonance frequency. In the following case, we assume the junction inductance and

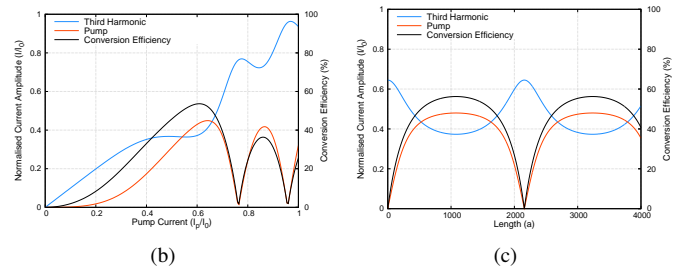
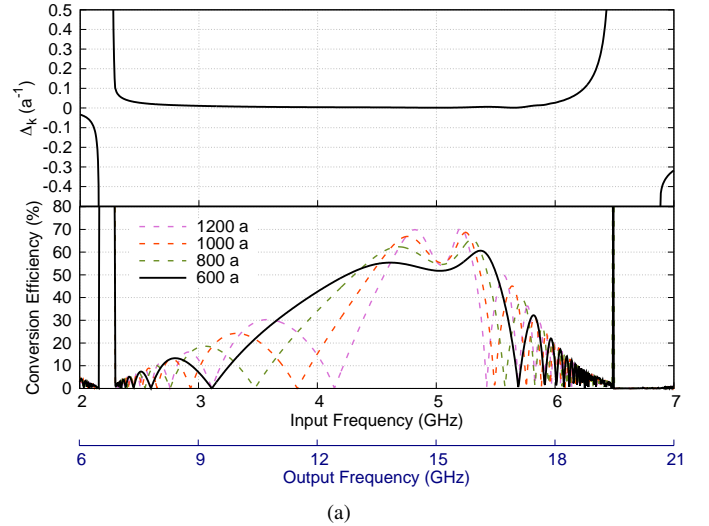


Fig. 5. (a) Top panel: Phase mismatched between the pump and the third harmonic. In this case, the resonator parameters were set to be $C_R = 4.6$ fF and $L_R = 41.3$ nH, giving resonances around 2.2 GHz and 6.6 GHz. Here, it is clearly seen that by lowering the Q-factor of the resonator circuit, we managed flatten the Δ_k curve approaching zero in between the two resonance frequencies. Bottom panel: This broaden the operational bandwidth of the third harmonic generator, with higher than 40% conversion efficiency from about 4–5.5 GHz. The asymmetry in the conversion curve was due to the the Q-factor of the 2.2 GHz resonance is naturally higher than the 6.6 GHz resonance. These plots were made by using $x = 600a$ and $I_p/I_0 = 0.645$. (b) The normalised amplitude of the resulting pump and third harmonic wave relative to the critical current of the Josephson junction (I_0), in relation with the strength of input pump current (I_p) with $f_p = 5$ GHz. (c) The normalised amplitude of the resulting pump and third harmonic wave along the transmission line.

capacitance is much smaller than the previous case, and by shifting the junction resonance upward in frequency, we show in Fig. 6 a similar broadband millimetre tripler can be realised using the same method presented above. In this case, the Josephson junction is resemblance more of an SIS junction with low junction capacitance.

For operation at even higher frequencies, into the sub-THz regime, the junction resonance need to be shifted to even higher frequency regime. This implies that the Josephson junction would needed to be replaced by a high current density SIS junction, such as NbN/AlN/NbN tunnel junction. The need for high current density junction here is three folds: to shift the junction resonance higher, to increase the Q-factor (therefore flatter dispersion curve at lower frequencies) and most importantly to improve the power handling. The latter requirement is due to the fact that the input pump wave cannot be stronger than the critical current density of the junction used to amplify the harmonic wave. Hence, there is a natural limit on the power handling of these devices.

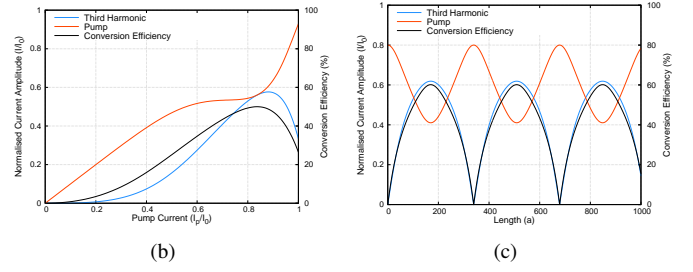
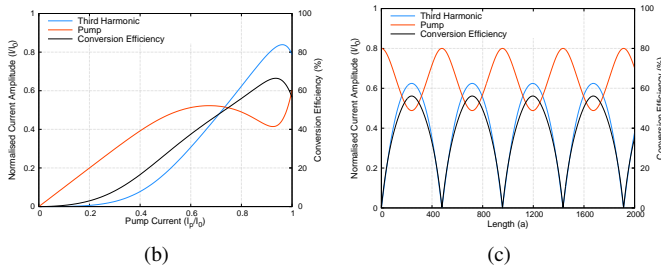
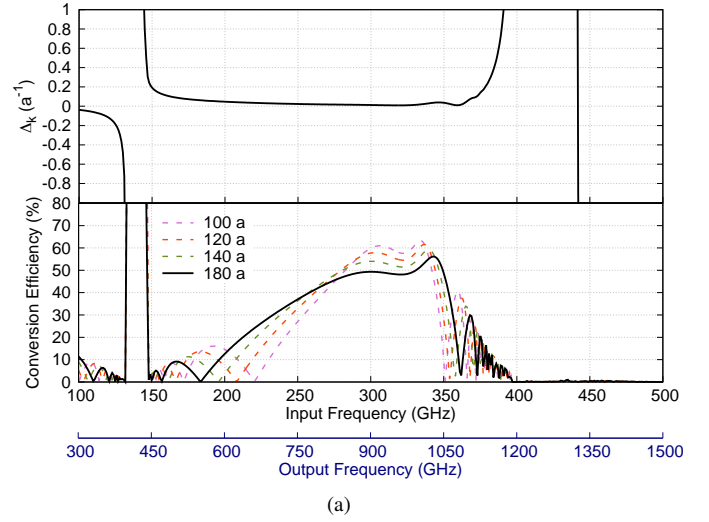
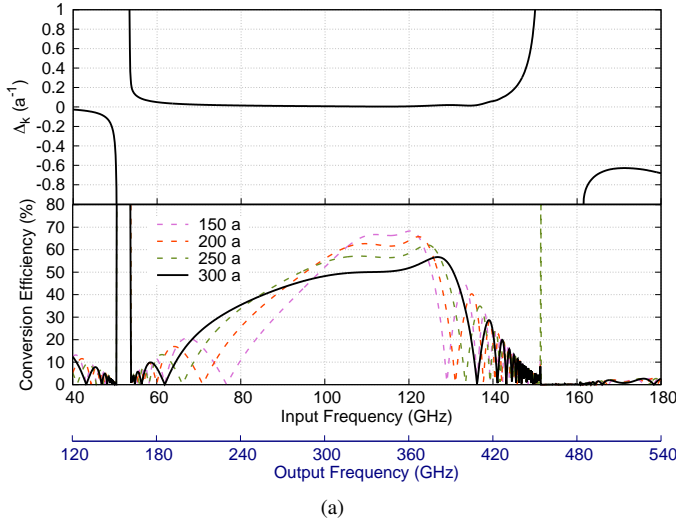


Fig. 6. (a) Top panel: Phase mismatched between the pump and the third harmonic. In this case, the junctions were set to be $C_j = 50$ fF, $L_j = 1$ pH, with $I_0 = 329$ μ A. The resonator parameters were set to be $C_R = 6.75$ fF and $L_R = 66$ pH, giving resonances around 50 GHz and 150 GHz. Here, it is clearly seen that by lowering the Q-factor of the resonator circuit, we managed to flatten the Δ_k curve approaching zero in between the two resonance frequencies. Bottom panel: This broadens the operational bandwidth of the third harmonic generator, with higher than 40% conversion efficiency from about 85–130 GHz. These plots were made by using $x = 250a$ and $I_p/I_0 = 0.8$. (b) The normalised amplitude of the resulting pump and third harmonic wave relative to the critical current of the Josephson junction (I_0), in relation with the strength of input pump current (I_p) with $f_p = 100$ GHz. (c) The normalised amplitude of the resulting pump and third harmonic wave along the transmission line.

Fig. 7. (a) Top panel: Phase mismatched between the pump and the third harmonic. In this case, the junctions were set to be $C_j = 50$ fF, $L_j = 0.22$ pH, with $I_0 = 1.5$ mA. The resonator parameters were set to be $C_R = 0.45$ fF and $L_R = 15.42$ pH, giving resonances around 150 GHz and 450 GHz. Here, it is clearly seen that by lowering the Q-factor of the resonator circuit, we managed to flatten the Δ_k curve approaching zero in between the two resonance frequencies. Bottom panel: This broadens the operational bandwidth of the third harmonic generator, with higher than 40% conversion efficiency from about 250–350 GHz. These plots were made by using $x = 100a$ and $I_p/I_0 = 0.8$. (b) The normalised amplitude of the resulting pump and third harmonic wave relative to the critical current of the Josephson junction (I_0), in relation with the strength of input pump current (I_p) with $f_p = 300$ GHz. (c) The normalised amplitude of the resulting pump and third harmonic wave along the transmission line.

This is illustrated in Fig. 7. Here we assume a junction current density of 75 kA/cm², 2 μ m² junctions, resulting in $I_0 = 1.5$ mA and $L_j = 0.22$ pH. This current density value is possible to achieve using a full NbN tunnel junction with AlN barrier [16]. In this example, we show that it is possible to convert more than 40% of the pump energy to generate and amplify the third harmonic wave from 750–1050 GHz, an extremely broadband operation for a tripler operating at this frequency range.

VI. THZ LO CHAIN

Although the above two examples show that it is possible to achieve a broadband tripler in mm and sub-mm wavelength, the power handling capability of these devices is still rather limited. This is due to the fact that the junction would lose its superconductivity above the critical current value of the junction I_0 . Furthermore, although the conversion efficiency is very high, between 40–70%, it is very sensitive to the input power of the pump wave. This can be seen clearly from

Fig. 6(b) and Fig. 7(b). To achieve such high conversion efficiency, the pump current needs to be at least $0.6I_0$. Therefore, if the first tripler is capable of convert only 40% of the pump power to the third harmonic wave, which in turn used to feed into the second tripler, this input power would be much less than $0.4I_0$. Hence the conversion efficiency drops significantly. Therefore, to construct a fully operational THz LO using the two TWPAMs with a W-band pump input, the two triplers need to be designed in sync.

Fig. 8(a) shows an example of a full THz LO chain using two TWPAMs along with a W-band signal generator. The junctions and resonators parameters were altered from the example given earlier, in order to achieve decent conversion efficiency in the final stage of the frequency conversion. In this case, the conversion efficiency of the 300 GHz tripler is maximised to about 80%, with a penalty on a slightly narrower operational bandwidth. The output power from this tripler is then used to feed the 900 GHz tripler. As can be seen, with this combination, we are able to generate close to $0.5I_0$ of

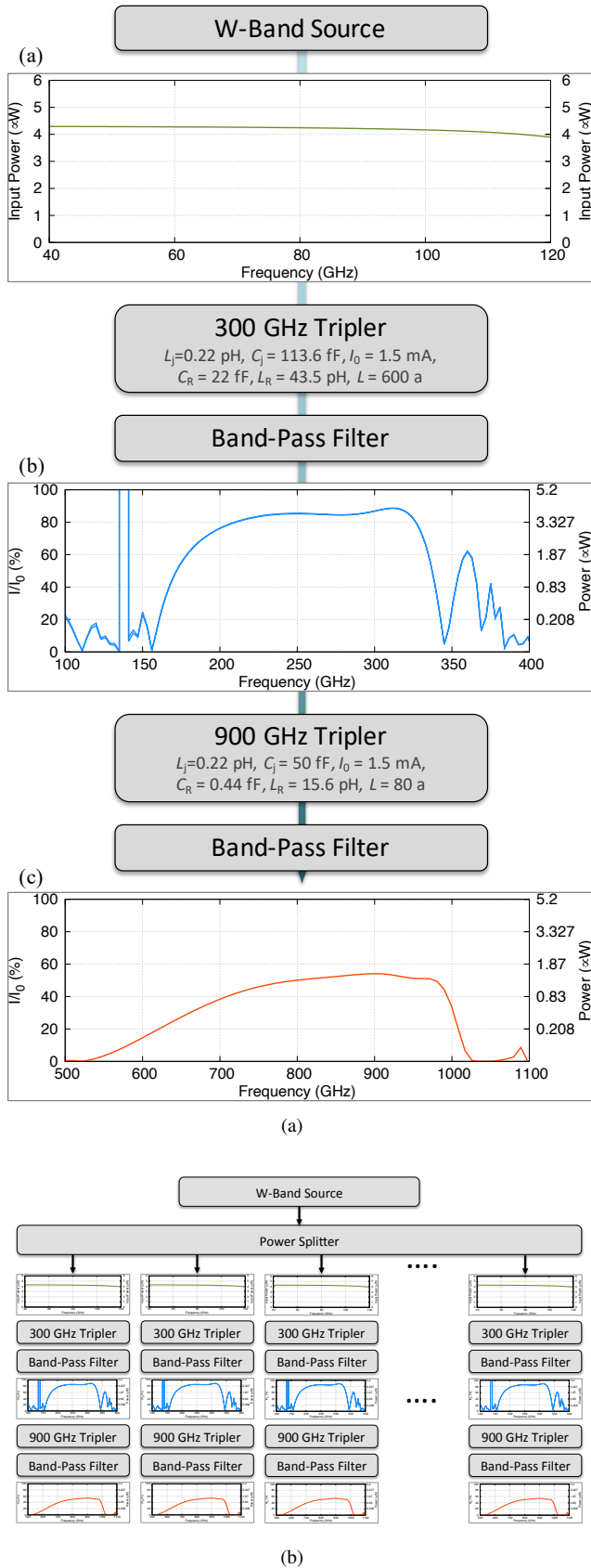


Fig. 8. (a) An example showing how the 300 GHz and 900 GHz tripler can be designed such that a maximum power output at the THz regime can be achieved with broadband operation. In this case, the output power is about $0.5I_0$, or in other words, it can be used to pump an SIS mixer up to half of its critical current value. (b) Diagram illustrating how a single W-band source can be used to feed multiple THz LO chain build using these TWPAMs.

output power from 700–1000 GHz. This is roughly equivalent to about $1.5 \mu\text{W}$ of output power, enough to pump an SIS mixer for heterodyne mixing operation in an astronomical instrument. Although one could argue that this scheme can only be used to feed a single SIS mixer, but the fact that the input power used here is negligible for any W-band source, a single W-band source can therefore be used to feed many of these LO chain, as shown in Fig. 8 (b). Noted that these planar circuit devices are much smaller than the traditional semiconductor frequency multiplier, and they can be fabricated with mass production. Hence, they can be incorporate along with the detector circuit, housed within the cryogenic system, with only a single W-band source to feed all the mm/sub-mm mixers.

CONCLUSION

We have presented an innovative method for developing a superconducting frequency multiplier using the TWPA technology. The travelling wave parametric tripler have a broad operational bandwidth with close to 50% conversion efficiency. They are compact in size, produce negligible heat and can be easily reproduce with standard planar circuit lithography technique. We have shown that the same technology can be use for designing low noise triplers in microwave, millimetre and sub-millimetre frequency regime. These triplers can also be cascaded together to construct a compact planar circuit THz LO chain which could be housed within the same block as the SIS mixer, or potentially integrated directly with the mixer's superconducting circuits.

ACKNOWLEDGMENT

This research was funded in part by the European Research Council (ERC) under the European Union's Horizon 2020 research and innovation programme with grant agreement No. [803862] (Project SPA4AstroQIT) and the MERAC Foundation. For the purpose of Open Access, the author has applied a CC BY public copyright license to any Author Accepted Manuscript version arising from this submission.

REFERENCES

- [1] J. Hesler, H. Song, and T. Nagatsuma, "Terahertz schottky diode technology," in *Handbook of terahertz technologies: Devices and applications*. Pan Stanford Publishing, 2015, no. 5, pp. 104–131.
- [2] I. Mehdi, J. V. Siles, C. Lee, and E. Schlecht, "Thz diode technology: Status, prospects, and applications," *Proceedings of the IEEE*, vol. 105, no. 6, pp. 990–1007, 2017.
- [3] M. S. Vitiello and A. Tredicucci, "Physics and technology of terahertz quantum cascade lasers," *Advances in Physics: X*, vol. 6, no. 1, p. 1893809, 2021.
- [4] A. Delga, "Quantum cascade detectors: A review," *Mid-infrared Opto-electronics*, pp. 337–377, 2020.
- [5] A. Leitenstorfer, A. S. Moskalenko, T. Kampfrath, J. Kono, E. Castro-Camus, K. Peng, N. Qureshi, D. Turchinovich, K. Tanaka, A. G. Markelz *et al.*, "The 2023 terahertz science and technology roadmap," *Journal of Physics D: Applied Physics*, vol. 56, no. 22, p. 223001, 2023.
- [6] J. D. Garrett, H. Rashid, G. Yassin, V. Desmaris, A. B. Pavolotsky, and V. Belitsky, "A nonlinear transmission line model for simulating distributed sis frequency multipliers," *IEEE Transactions on Terahertz Science and Technology*, vol. 10, no. 3, pp. 246–255, 2020.

- [7] H. Rashid, S. Krause, D. Meledin, V. Desmaris, A. Pavolotsky, and V. Belitsky, "Frequency multiplier based on distributed superconducting tunnel junctions: Theory, design, and characterization," *IEEE Transactions on Terahertz Science and Technology*, vol. 6, no. 5, pp. 724–736, 2016.
- [8] C. Macklin, K. O'Brien, D. Hover, M. Schwartz, V. Bolkhovskiy, X. Zhang, W. Oliver, and I. Siddiqi, "A near-quantum-limited josephson traveling-wave parametric amplifier," *Science*, vol. 350, no. 6258, pp. 307–310, 2015.
- [9] B. H. Eom, P. K. Day, H. G. LeDuc, and J. Zmuidzinas, "A wideband, low-noise superconducting amplifier with high dynamic range," *Nature Physics*, vol. 8, no. 8, pp. 623–627, 2012.
- [10] L. Planat, A. Ranadive, R. Dassonneville, J. Puertas Martínez, S. Léger, C. Naud, O. Buisson, W. Hasch-Guichard, D. M. Basko, and N. Roch, "Photonic-crystal josephson traveling-wave parametric amplifier," *Physical Review X*, vol. 10, no. 2, p. 021021, 2020.
- [11] K. O'Brien, C. Macklin, I. Siddiqi, and X. Zhang, "Resonant phase matching of josephson junction traveling wave parametric amplifiers," *Physical review letters*, vol. 113, no. 15, p. 157001, 2014.
- [12] T. White, J. Mutus, I.-C. Hoi, R. Barends, B. Campbell, Y. Chen, Z. Chen, B. Chiaro, A. Dunsworth, E. Jeffrey *et al.*, "Traveling wave parametric amplifier with josephson junctions using minimal resonator phase matching," *Applied Physics Letters*, vol. 106, no. 24, 2015.
- [13] J. M. Navarro and B.-K. Tan, "Optimising the design of a broadband josephson junction twpa for axion dark matter search experiments," in *Quantum Technology: Driving Commercialisation of an Enabling Science II*, vol. 11881. SPIE, 2021, pp. 139–148.
- [14] J. N. Montilla and B.-K. Tan, "Design of high compression point josephson junction travelling wave parametric amplifiers for readout of millimetre and sub-millimetre astronomical receivers," in *Millimeter, Submillimeter, and Far-Infrared Detectors and Instrumentation for Astronomy XI*, vol. 12190. SPIE, 2022, pp. 1244–1253.
- [15] O. Yaakobi, L. Friedland, C. Macklin, and I. Siddiqi, "Parametric amplification in josephson junction embedded transmission lines," *Physical Review B*, vol. 87, no. 14, p. 144301, 2013.
- [16] Z. Wang, A. Kawakami, A. Saito, and K. Hamasaki, "1/f noise in high current density nbn/aln/nbn tunnel junctions," *IEEE transactions on applied superconductivity*, vol. 11, no. 1, pp. 84–87, 2001.